Even though the proton transfer probably proceeds through hydrogen-bonded complexes, addition of CF_3^- to the carbonyl group may occur on some collisions, yielding enolate ion 3 directly. This is not a productive pathway, in the sense that it is simply reversible (at low pressure) formation of a nonreacting intermediate, so it cannot affect the apparent rate of reaction 7. It may influence the dynamics, however, in that the total lifetime of all the intermediates will be greater than if the enolate were not a feature on the potential surface. One might therefore expect to observe a lower pressure onset for third-body stabilization reactions of $CF_3COCH_2^-$ than for intermediates of other proton-transfer reactions.

Given that trifluoroacetone enolate branches in these photochemical reactions, one might expect methyl acetate enolate to do the same, but it does not. This is probably caused by two factors. First, the resonant mode in 4 is probably a weaker absorption than the intense C–F stretching mode that is undoubtedly being pumped in the decomposition of 3. The absorption rate constants are thus smaller, and decomposition occurs before the ion has been pumped far above threshold. Second, the difference between channels is 6 kcal/mol greater than that for dissociation of 3. The results of the photolyses of 1 and 5 indicate how quickly the rate constant for decomposition may increase with increasing energy; it is not unreasonable that no branching occurs if this process also involves an intermediate whose lowest threshold energy decomposition pathway yields $HCCO^-$. Furthermore, if the large difference in reaction efficiency between reactions 7 and 12 does not simply reflect their relative exothermicities, then CF_3^- has a larger barrier to proton transfer from ketene than methoxide does and is therefore less likely to react via the lower decomposition channel.

The total dissociation yield, even in branching systems, should depend primarily on fluence rather than intensity,[34] and this holds true for the decompositions of 2 and 3. Plots of –ln (fraction undecomposed) vs. fluence are linear if steady-state energy distributions are formed during irradiation;[35] data for ion 2 are linear when depicted in such a plot. This suggests that if ion 2 exists as two asymmetric hydrogen-bound isomers that interconvert extremely slowly,[2] the two complexes absorb infrared photons at identical rates. Subpopulations that are pumped at different rates

yield bent fluence curves.[22,23] A small intensity effect on total yield is observed in the photolysis of 3, however. We infer that there is a modest bottleneck in the pumping process, so that the total energy absorption is slightly intensity dependent. Intensity effects on dissociation yield are strongly dependent on the particular molecules involved; some species show no effects[36] and some show large ones.[37,38]

Conclusions

Insofar as the aforementioned results represent general phenomena, several conclusions may be drawn. First, on the basis of the observed photochemical behavior of ion 2 and on subsequent additional work, we conclude[29] that the currently accepted values of the relative gas-phase acidities of alcohols and HF are in error by approximately 2.2 kcal/mol. Second, on the basis of the observed branching behavior of ion 3 and available kinetic data on four-center elimination reactions, we conclude that proton transfers do not proceed by addition–elimination reactions even when the addition complex is a very stable species on the potential-energy surface. Finally, an ion decomposing to elimination products need not do so directly but can decompose to an ion-molecule complex and then transfer a proton within the complex. This mechanism has been previously suggested for positive ion systems.[39–42]

Registry No. CH_3O^-, 3315-60-4; t-BuOH, 75-65-0; F^-, 16984-48-8; t-BuCH$_2$OH, 75-84-3; CF_3^-, 54128-17-5; H_2CCO, 463-51-4.

(34) Thiele, E.; Goodman, M. F.; Stone, J. Chem. Phys. Lett. 1980, 72, 34–38.
(35) Quack, M. J. Chem. Phys. 1979, 70, 1069–1071.

(36) Black, J. G.; Yablonovitch, E.; Bloembergen, N. Phys. Rev. Lett. 1977, 38, 1131–1134.
(37) King, D. S.; Stephenson, J. C. Chem. Phys. Lett. 1979, 66, 33–38.
(38) Simpson, T. B.; Mazur, E.; Lehmann, K. K.; Burak, I.; Bloembergen, N. J. Chem. Phys. 1983, 79, 3373–3381.
(39) Bowen, R. D.; Stapleton, B. J.; Williams, D. H. J. Chem. Soc., Chem. Commun. 1978, 24–26.
(40) Morton, T. H. J. Am. Chem. Soc. 1980, 102, 1596–1602.
(41) Longevialle, P.; Botter, R. J. Chem. Soc., Chem. Commun. 1980, 823–825.
(42) Moylan, C. R.; Brauman, J. I. J. Am. Chem. Soc. in press.

Origin of the Temperature-Dependent Product Variation in Carbene Reaction with Alcohol

Setsuko Oikawa* and Minoru Tsuda

Contribution from the Laboratory of Physical Chemistry, Pharmaceutical Sciences, Chiba University, Chiba 260, Japan. Received August 21, 1984

Abstract: Extraordinarily temperature-dependent product variation in the reaction of carbene with alcohol has been investigated by ab initio MO theoretical calculations of the potential energy barrier along the IRC (intrinsic reaction coordinate) path on the hypersurface. The classical rate constants along the one-dimensional IRCs were calculated and compared with those including a quantum-mechanical tunneling effect. The extraordinary observation originates from the stable intermediate formation at low temperatures in the singlet carbene insertion reaction into the O–H bond of alcohols. The contribution of the triplet carbene is not important. The classical mechanism and the tunneling gave the same conclusion. The normal mode of vibration of imaginary frequency at the saddle point is approximately the displacement of a hydrogen atom only in all the reactions investigated. However, not only the hydrogen atom displacement but also the whole structure change along the IRC path contribute to the tunneling process.

I. Introduction

A few years ago, Tomioka and Izawa reported an extraordinarily temperature-dependent product variation in the reaction of carbene with alcohol; i.e., irradiation of phenyldiazomethane

(1) in degassed 2-propanol in a quarz tube at 20 °C gave 2-propyl benzyl ether (77%) as a main product (O–H insertion), but irradiation of 1 in frozen 2-propanol matrix at –196 °C gave the C–H insertion products in high yield (78%) with a sharply reduced

Product Variation in Carbene Reaction with Alcohol

J. Am. Chem. Soc., Vol. 107, No. 7, 1985 1941

yield of the ether (15%). Similar results were obtained in the cases of methanol and ethanol instead of 2-propanol.[1] To explain this remarkable phenomenon they proposed a tunneling mechanism for the hydrogen abstraction by triplet carbene.[2]

There are a few experiments on tunneling in the low-temperature limit. Senthilnathan and Platz measured the absolute decay rate of diphenylcarbene at 77–113 K and concluded that the predominant carbene decay pathway is by hydrogen atom tunneling through a small barrier.[3] Sprague and Williams reported hydrogen atom abstraction from solid acetonitrile at 77–87 K with an activation energy of 1.4 ± 0.1 kcal/mol,[4] which is much smaller than the value 10.0 ± 0.5 kcal/mol for the same reaction occurring in the gas phase at 373–573 K.[5] Le Roy et al. performed one-dimensional tunneling calculations for hydrogen abstraction and concluded that at 77–87 K the reaction proceeds almost totally via quantum-mechanical tunneling.[6] Siebrand et al.[7] and McKinnon et al.[8] also investigated the temperature dependence of the hydrogen tunneling reaction rate recently. Brunton et al. measured the rate constants for the isomerization of 2,4,6-tri-*tert*-butylphenol to 3,5-di-*tert*-butylneophenyl from −26 to −160 °C and explained the result by quantum-mechanical tunneling[9] using Le Roy's procedure based on the one-dimensional barrier.[6]

However, no real information on the potential energy surface is known for these reactions. A simple Eckart-, parabolic-, or Gaussian-type one-dimensional surface was postulated in these papers. In the present paper, $3N - 6$ dimensional potential energy hypersurfaces, where N is the number of atoms constructing the reaction system, have been calculated by an ab initio MO method for the insertion reaction into the O–H or the C–H bond of methanol by singlet methylene as well as the hydrogen abstraction reaction from the same bonds by triplet methylene. The rate constant of a chemical reaction is the probability that the representative point of the reaction system migrates from a potential energy minimum corresponding to the reactant into the other minimum corresponding to the product on the potential energy hypersurface of the reaction system. When mass-weighted Cartesian coordinates are used in the construction of the hypersurface, the mass of the representative point becomes unity. The intrinsic reaction coordinate (IRC),[10] the lowest energy path of a chemical reaction on the hypersurface, gives the potential energy barrier of the smallest thickness among the possible reaction paths passing through the saddle point. Therefore, the upper limit of the relative rate constant may be estimated when the reaction occurs by tunneling as well as a classical mechanism, if the one-dimensional model calculation of the rate constant is performed with the potential barrier along the IRC.

II. Potential Energy Hypersurface and Activation Energy

Method of Calculations. Ab initio RHF and UHF MO methods were adapted for a singlet and a triplet reaction system, respectively. In the UHF calculation, contamination from higher multiplicity is excluded from electron densities by the method of projection operator.[11] Basis sets used are STO-3G and 6-31G**. In the latter, a set of six d-like functions (x^2, y^2, z^2, xy, yz, zx times $\exp(-\alpha r^2)$, $\alpha = 0.8$) is centered on carbon and oxygen, and a set of three p-type functions is centered on hydrogen ($\alpha = 1.1$),

Table I. Total Energies (au) and Activation Energies (kcal/mol) of the Reaction System at the Optimized Geometries[a]

molecules		6-31G**	STO-3G
Reactant and Product			
CH_2 (singlet)	C_{2v}	−38.87631	−38.37230
CH_2 (triplet)	C_{2v}	−38.91258	−38.43623
CH_3OH	C_s	−115.04671	−113.54919
C_2H_5OH	C_s	−154.09016	−152.13267
CH_3OCH_3	C_s	−154.07008	−152.12929
$\cdot CH_3$ (doublet)	D_{3h}	−39.56446	−39.07701*
$\cdot CH_2OH$ (doublet)	C_s	−114.41728	−112.91357
$CH_3O\cdot$ (doublet)	C_s	−114.42558	−112.96089
Reacting Molecules			
insertion			
O–H IM	C_1	−153.93668	−151.96334
O–H SP	C_1	−153.91611	−151.92907
C–H SP	C_1	−153.91186	−151.89689
abstraction			
O–H SP	C_s	−153.93629	−151.97288
C–H SP	C_s	−153.93296	−151.95000
Activation Energies ($\Delta E^{+\circ}$)			
insertion			
O–H (high temp)		4.33	−4.75
O–H (low temp)		12.91	21.51
C–H		7.00	15.44
abstraction			
O–H		22.53	7.87
C–H		24.62	22.23

[a] SP, saddle point. IM, intermediate. An asterisk indicates C_{3v} structure, which is more stable than D_{3h} in STO-3G.

in addition to the standard split valence contracted GTO set.[12] The structures of the reaction system at stationary points on the potential energy hypersurface, the minimum and the saddle points, were fully optimized at the self consistent field (SCF) level of theory in each case of basis sets and analyzed in terms of their harmonic vibrational frequencies. The potential energies at the stationary points were used for the determination of activation energies of reactions. Computer programs used were GAUSSIAN80[13] for geometry optimization and GAMESS[14] for vibrational analysis, respectively. The IRC was calculated by the steepest descent path determination,[15] starting from the saddle point toward two directions following the normal mode of vibration having an imaginary frequency. The computer program for the IRC is homemade, utilizing GAUSSIAN80 in the energy and energy gradient calculations.

Potential Energy Barriers. Sections of the potential energy hypersurface following the IRC paths of the four elementary reactions are shown in Figure 1, which are the results of 6-31G** SCF calculations. Total energies of the reaction systems at all of the stationary points are collected in Table I. The outstanding characteristic in the potential energy hypersurface of Figure 1a is the stable intermediate formation in the process of the singlet carbene insertion into the O–H bond. This type of potential energy hypersurface is responsible to the temperature dependence of product variation, because the representative point of the reaction system has enough kinetic energy to pass over the saddle point at high temperatures but the point is effectively trapped at the potential minimum corresponding to the stable intermediate at low temperatures; i.e., the singlet carbene insertion into the O–H bond takes place easily in higher temperatures but the stable

(1) H. Tomioka and Y. Izawa, *J. Am. Chem. Soc.* **99**, 6128 (1977).

(2) Y. Izawa and H. Tomioka, *Photochemistry (Kohkagaku in Japanese)* **7**, 43 (1983).

(3) U. P. Senthilnathan and M. S. Platz, *J. Am. Chem. Soc.* **102**, 7637 (1980).

(4) E. D. Sprague, and F. Williams, *J. Am. Chem. Soc.*, **93**, 787 (1971).

(5) M. H. J. Wijnern, *J. Chem. Phys.*, **22**, 1074 (1954).

(6) (a) R. J. Le Roy, E. D. Sprague, and F. Williams, *J. Phys. Chem.* **76**, 546 (1972). (b) R. J. Le Roy, H. Murai, and F. Williams, *J. Am. Chem. Soc.*, **102**, 2325 (1980).

(7) W. Siebrand, T. A. Wildman, and M. Z. Zgierski, *Chem. Phys. Lett.*, **98**, 108 (1983).

(8) W. R. McKinnon and C. M. Hurd, *J. Phys. Chem.*, **87**, 1283 (1983).

(9) (a) G. Brunton, D. Griller, L. R. C. Barclay, and K. U. Ingold, *J. Am. Chem. Soc.*, **98**, 6803 (1976). (b) G. Brunton, J. A. Gray, D. Griller, L. R. C. Barclay, and K. U. Ingold, *J. Am. Chem. Soc.*, **100**, 4197 (1978).

(10) (a) K. Fukui, *J. Phys. Chem.*, **74**, 4161 (1970). (b) K. Fukui, S. Kato, and H. Fujimoto, *J. Am. Chem. Soc.*, **97**, 1 (1975).

(11) (a) T. Amos and L. C. Snyder, *J. Chem. Phys.*, **41**, 1773 (1964). (b) L. C. Snyder and T. Amos, *J. Chem. Phys.*, **42**, 3670 (1965).

(12) P. C. Hariharan and J. A. Pople, *Theor. Chim. Acta*, **28**, 1 (1971).

(13) J. S. Binkey, R. A. Whiteside, R. Krishnan, R. Seeger, D. J. DeFrees, H. B. Schlegel, S. Topiol, L. R. Kahn, and J. A. Pople, *QCPE*, **13**, 406 (1981).

(14) M. Dupuis, D. Spangler, J. J. Wendoloski, NRCC Software Catalog: QG01 "GAMESS".

(15) K. Ishida, K. Morokuma, and A. Komornicki, *J. Chem. Phys.*, **66**, 2153 (1977).

(16) S. W. Benson, "Thermochemical Kinetics", 2nd ed., Wiley, New York, 1976. L. B. Harding, H. B. Schlegel, R. Krishnan, and J. A. Pople, "Potential Energy Surface and Dynamic Calculations", D. G. Truhler Ed., Plenum, New York, 1981, p 178.

(17) S. Oikawa and M. Tsuda, unpublished work.
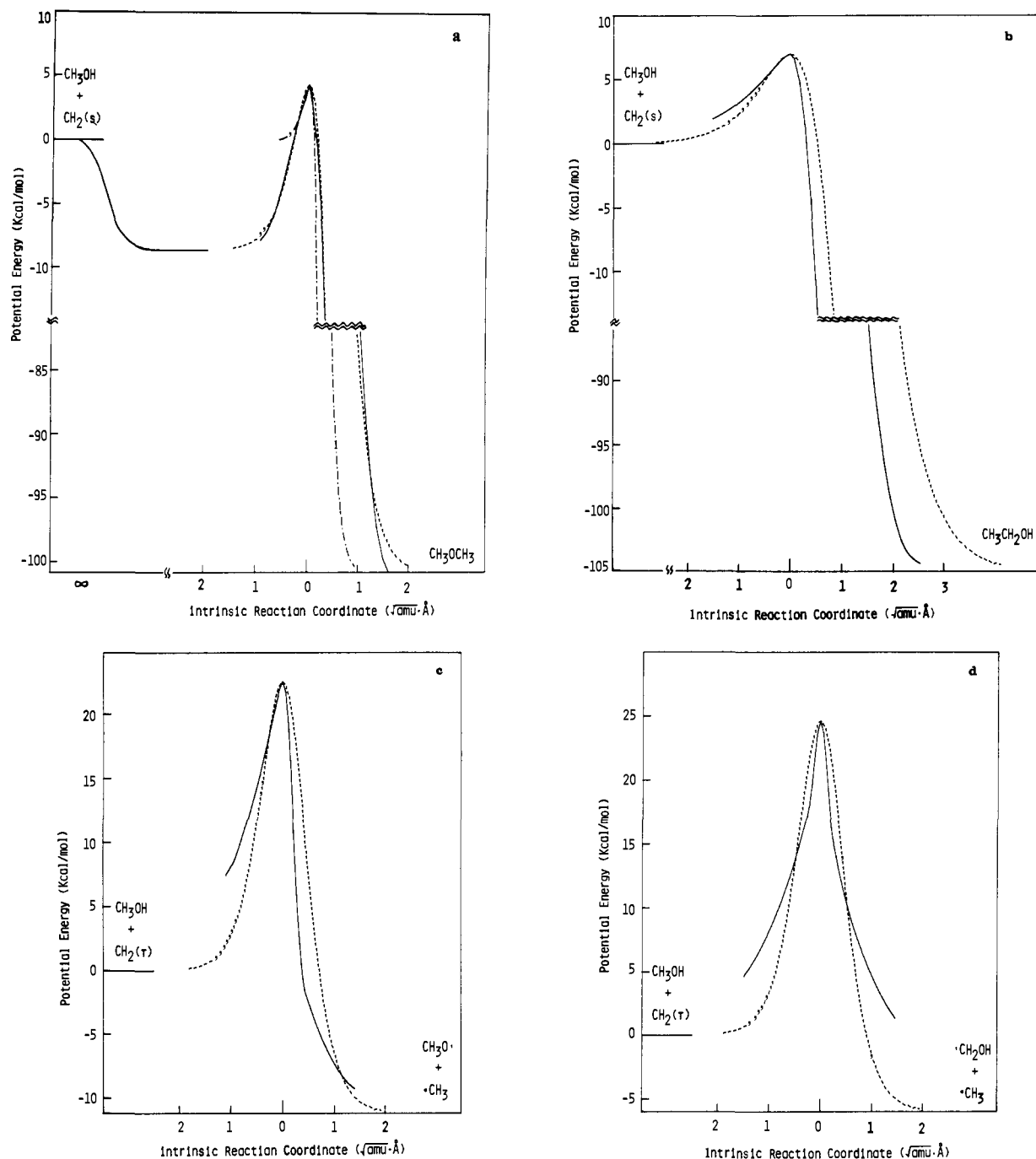
(18) C. Eckart, *Phys. Rev.*, **35**, 1303 (1930).

Figure 1. Sections of the potential energy hypersurface following the IRC path in the reaction of methylene with methanol: (a) insertion to O–H bond by singlet methylene, (b) insertion to C–H bond by singlet methylene; (c) hydrogen abstraction from O–H bond by triplet methylene; (d) hydrogen abstraction from C–H bond by triplet methylene; (---) Eckart potential, (···) (in part a) Eckart potential which starts from the initial reactants (see text, Section IV).

intermediate formation blocks the insertion reaction in low temperatures. On the other hand, singlet carbene insertion into a C–H bond and hydrogen abstraction by a triplet carbene from both O–H and C–H bonds proceed in a simple or normal fashion as shown in Figure 1, parts b–d; i.e., no stable intermediate is produced in these reaction processes.

The potential energy hypersurface following the IRC path has qualitatively the same profile independent of basis sets in each of the four elementary reactions except for the hydrogen abstraction from the O–H bond, where the activation energy calculated by STO-3G is very small compared with the value obtained by 6-31G**. This discrepancy comes from the fact that the $CH_3O\cdot$ radical is extremely stable relative to the $\cdot CH_2OH$ radical in the STO-3G calculation. In the 6-31G** calculation, the energies of these two radicals are approximately equal in accordance with experiment.[13]

Activation Energies. The activation energies in both hydrogen abstractions from C–H and O–H bonds are substantially the same: i.e., 24.6 and 22.5 kcal/mol, respectively (Table I). The values are very large compared with those of the insertion reaction into C–H and O–H bonds: i.e., 7.0 and 4.33 (at high temperatures) or 12.9 (at low temperature) kcal/mol, respectively. Therefore, the contribution of the triplet carbene is not important in the classical mechanism. It should be kept in mind, however, that the insertion into and the hydrogen abstraction from C–H bonds have three times as large a chance of reaction as those into and from O–H bonds, respectively.

III. Potential Energy and Structure at the Saddle Point

The structures of the reaction system at the saddle points are shown in Figure 2 as well as that of the intermediate produced in the O–H insertion process. Details of the geometries are

Product Variation in Carbene Reaction with Alcohol

J. Am. Chem. Soc., Vol. 107, No. 7, 1985 1943

collected in Table II.

Determination of the Structure at the Saddle Point in Insertion.
In another work on the insertion of singlet methylene in the C–H
bond of methane, two kinds of saddle points were found; one
corresponds to the cis conformation having 18.9 kcal/mol lower
potential energy than that corresponding to the trans conforma-
tion.[17]
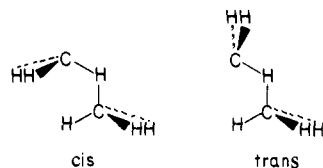
Each conformation has a unique normal mode of vibration of
imaginary frequency. Because of the large difference of potential
energy between the two saddle points, only the cis conformation
was considered in this research as shown in Figure 2, a_2 and b.

The structures of the reaction system at the saddle points form
a triangle constructed by the O–H or C–H bond to be inserted
at a carbon atom of methylene. The triangle bisects the plane
containing the three atoms of methylene. The triangle produced
at the saddle point in the insertion process into the C–H bond of
methanol has two C–H bonds of an approximately equal distance,
18.4% longer than that of methanol itself (Figure 2b), but the
O–H bond length of the triangle in Figure $2a_2$, which is 15.8%
longer than that of methanol, is shorter than the C–H distance
reflecting the property of heterocycles.

The displacement of the atoms in the direction of the arrows
shown in Figure 2, parts a_2 and b, which corresponds to the unique
normal mode of vibration of imaginary frequency at the saddle
point, produces dimethyl ether and ethanol, respectively.

Structure at the Saddle Point in Abstraction. In abstraction
reactions, a hydrogen atom bridge is formed at the saddle point
between the attacking methylene and the hydrogen atom of the
C–H or O–H bond (Figure 2, parts c and d). In the former the
bond lengths of the breaking and forming C–H bonds are nearly
equal and 22.4% longer than the equilibrium distance of the C–H
bond in methanol. In the latter, the breaking O–H bond length
is shorter than the forming C–H bond distance. But the breaking
bond is 23.2% longer than the equilibrium one, i.e., the same
lengthening ratio as that in C–H abstraction. This interesting
phenomenon may be characteristic for the R–H bond breaking
by hydrogen abstraction. In Figure 2, parts c and d, the dis-
placement of the bridged hydrogen atom along the direction of
the arrow produces ·CH₃ and ·CH₂OH and ·CH₃ and CH₃O·,
respectively.

IV. Rate Constant of the Reaction along the IRC Path

Potential Energy Barrier Fitting with a Mathematical Function.
A number of investigations of tunneling effects in chemical re-
actions have employed one-dimensional potential energy barriers
of the Eckart or Bell type, for which the permeabilities can be
given in analytical form.[6,7,19,20] In the present paper, the IRC
potential energy barriers of Figure 1 are approximately fitted with
the Eckart-type potential. The asymmetric Eckart potential $V(Q)$
along with the reaction coordinate Q is written as[18]

$$V(Q) = \Delta H \xi/(1 - \xi) - P^2/(1 - \xi)^2 \qquad (1)$$

with $\xi = \exp(2\pi Q/L)$, $P = V(Q_m)^{1/2} + (V(Q_m) + \Delta H)^{1/2}$, $Q_m = (L/2\pi) \ln [(P^2 - \Delta H)/(P^2 + \Delta H)]$, and $V(Q_m) = (P^2 - \Delta H)^2/4P^2$,
where $\Delta H = V(+\infty) - V(-\infty)$ is the exothermicity of the reaction,
$V(Q_m)$ is the barrier height measured from the reactant, and L
is a characteristic length related to the tunneling frequency.

In the curve fitting of the IRC potential of Figure 1, with the
Eckart-type potential, the position of the saddle point is $Q = Q_m$,
that of the reactant $Q = -\infty$, and that of the product $Q = +\infty$.
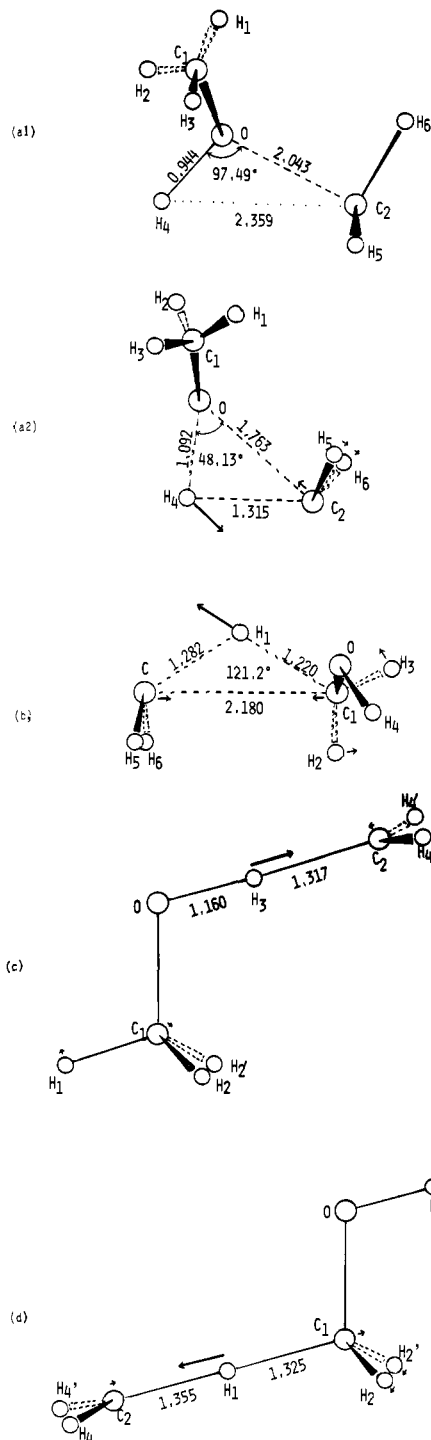L was calculated from formula 1 with the condition that the

(19) W. Jakubetz, *J. Am. Chem. Soc.*, **101**, 298 (1979).
(20) D. G. Truhlar and A. Kuppermann, *J. Am. Chem. Soc.*, **93**, 1840 (1971).

Figure 2. Optimized structures of saddle points and intermediates: (a_1)
intermediate in O–H insertion, (a_2) saddle point in O–H insertion, (b)
saddle point in C–H insertion, (c) saddle point in O–H abstraction, (d)
saddle point in C–H abstraction. The arrows show the normal mode of
vibration of imaginary frequency at the saddle point. The numerals are
typical bond lengths (Å) and bond angles (deg). Details of the geome-
tries are collected in Table II.

half-value width of the potential barrier curve has the same value
in both the IRC and the Eckart potential. The result of curve
fitting is also shown in Figure 1, where the Eckart type potential
is the dotted curve.

Rate Constant Calculation. The representative point having
the translational energy (E_T) permeates through the Eckart po-
tential barrier with a probability $P(E_T)$.[18]

$$P(E_T) = 1 - \frac{\cosh[2\pi(a - b)] + \cosh[2\pi d]}{\cosh[2\pi(a + b)] + \cosh[2\pi d]} \qquad (2)$$

Table II. Optimized Geometries of the Reaction System
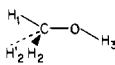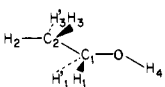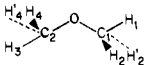
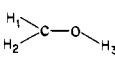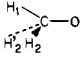| molecules	symmetry				(6-31G**)
		Reactant and Product			
CH_2 (singlet)	C_{2v}	$r(CH)$	1.099	$\angle(HCH')$	102.9
CH_2 (triplet)	C_{2v}	$r(CH)$	1.072	$\angle(HCH')$	131.2
CH_3OH	C_s	$r(CO)$	1.399	$\angle(H_1CO)$	107.4
		$r(CH_1)$	1.082	$\angle(H_2CO)$	112.1
		$r(CH_2)$	1.088	$\angle(H_3OC_1)$	109.7
		$r(OH_3)$	0.942	$\omega(H_2COH_1)$	118.7
C_2H_5OH	C_s	$r(C_1O)$	1.404	$\angle(C_2C_1O)$	108.1
		$r(C_1C_2)$	1.515	$\angle(H_1C_1O)$	110.7
		$r(C_1H_1)$	1.090	$\angle(H_2C_2O)$	110.6
		$r(C_2H_2)$	1.086	$\angle(H_3C_2C_1)$	110.3
		$r(C_2H_3)$	1.085	$\angle(H_4OC_1)$	109.9
		$r(OH_4)$	0.942	$\omega(H_1C_1OC_3)$	120.5
				$\omega(H_2C_2C_1H_3)$	120.2
CH_3OCH_3	C_s	$r(C_1O)$	1.392	$\angle(C_1OC_2)$	115.7
		$r(C_2O)$	1.398	$\angle(H_1C_1O)$	107.5
		$r(C_1H_1)$	1.082	$\angle(H_2C_1O)$	111.8
		$r(C_1H_2)$	1.089	$\angle(H_3C_2O)$	112.1
		$r(C_2H_3)$	1.087	$\angle(H_4C_2O)$	109.8
		$r(C_2H_4)$	1.086	$\omega(H_2C_1OC_2)$	119.1
				$\omega(H_4C_2OH_3)$	120.3
$\cdot CH_3$ (doublet)	D_{3h}	$r(CH)$	1.073		
$\cdot CH_2OH$ (doublet)	C_s	$r(CO)$	1.356	$\angle(H_1CO)$	115.6
		$r(CH_1)$	1.069	$\angle(H_2CO)$	120.5
		$r(CH_2)$	1.072	$\angle(H_3CO)$	110.6
		$r(OH_3)$	0.942		
$CH_3O\cdot$ (doublet)	C_s	$r(CO)$	1.383	$\angle(H_1CO)$	106.2
		$r(CH_1)$	1.089	$\angle(H_2CO)$	111.7
		$r(CH_2)$	1.086	$\omega(H_2C_1OH_3)$	117.9
		Reaction Molecules[a]			
insertion					
O-H IM	C_1	$r(C_1O)$	1.411	$\angle(H_3C_1O)$	110.5
		$r(C_1H_1)$	1.080	$\angle(H_4OC_1)$	109.6
		$r(C_1H_2)$	1.083	$\angle(C_2H_4O)$	59.1
		$r(C_1H_3)$	1.085	$\angle(H_5C_2H_4)$	82.4
		$r(OH_4)$	0.944	$\angle(H_6C_2H_4)$	113.9
		$r(C_2H_4)$	2.359	$\omega(H_2C_1OH_1)$	119.0
		$r(C_2H_5)$	1.096	$\omega(H_3C_1OH_1)$	-118.4
		$r(C_2H_6)$	1.096	$\omega(H_4OC_1H_1)$	176.7
		$\angle(H_1C_1O)$	107.0	$\omega(C_2H_4OC_1)$	114.6
		$\angle(H_2C_1O)$	110.8	$\omega(H_5C_2H_4O)$	105.8
				$\omega(H_6C_2H_4O)$	5.38
O-H SP	C_1	$r(C_1O)$	1.405	$\angle(H_3C_1O)$	108.8
		$r(C_1H_1)$	1.085	$\angle(H_4OC_1)$	112.8
		$r(C_1H_2)$	1.087	$\angle(C_2H_4O)$	93.7
		$r(C_1H_3)$	1.092	$\angle(H_5C_2H_4)$	116.6
		$r(OH_4)$	1.092	$\angle(H_6C_2H_4)$	119.9
		$r(C_2H_4)$	1.315	$\omega(H_2C_1OH_1)$	120.5
		$r(C_2H_5)$	1.079	$\omega(H_3C_1OH_1)$	-119.5
		$r(C_2H_6)$	1.081	$\omega(H_4OC_1H_1)$	230.5
		$\angle(H_1C_1O)$	109.5	$\omega(C_2H_4OC_1)$	101.9
		$\angle(H_2C_1O)$	111.3	$\omega(H_5C_2H_4O)$	69.5
				$\omega(H_6C_2H_4O)$	-69.0
C-H SP	C_1	$r(C_1O)$	1.375	$\angle(H_3C_1O)$	113.9
		$r(C_1H_1)$	1.220	$\angle(H_4OC_1)$	110.7
		$r(C_1H_2)$	1.073	$\angle(C_2H_1C_1)$	121.2
		$r(C_1H_3)$	1.087	$\angle(H_5C_2H_1)$	105.1
		$r(OH_4)$	0.944	$\angle(H_6H_1H_1)$	105.3
		$r(C_2H_1)$	1.282	$\omega(H_2C_1OH_1)$	130.8

Table II (Continued)

molecules	symmetry					(6-31G**)
C–H SP	C_1	$r(C_2H_5)$	1.088	$\omega(H_3C_1OH_1)$	-106.0
		$r(C_2H_6)$	1.086	$\omega(H_4OC_1H_1)$	50.0
		$\angle(H_1C_1O)$	108.7	$\omega(C_2H_1C_1O)$	97.8
		$\angle(H_2C_1O)$	109.1	$\omega(H_5C_2H_1C_1)$	63.8
				$\omega(H_6C_2H_1C_1)$	-50.2
abstraction					
O–H SP	C_s	$r(C_1O)$	1.400	$\angle(H_1C_1O)$	105.9
		$r(C_1H_1)$	1.085	$\angle(H_2C_1O)$	112.3
		$r(C_1H_2)$	1.086	$\angle(H_3OC_1)$	107.4
		$r(OH_3)$	1.160	$\angle(C_2H_3O)$	180.0
		$r(C_2H_3)$	1.317	$\angle(H_4C_2H_3)$	116.9
		$r(C_2H_4)$	1.073	$\omega(H_2C_1OH_1)$	118.2
				$\omega(H_4C_2H_3C_1)$	92.0
C–H SP	C_s	$r(C_1O)$	1.382	$\angle(H_1C_1O)$	105.5
		$r(C_1H_1)$	1.325	$\angle(H_2C_1O)$	114.6
		$r(C_1H_2)$	1.085	$\angle(H_3OC_1)$	110.3
		$r(OH_3)$	0.944	$\angle(C_2H_1C_1)$	180.0
		$r(C_2H_1)$	1.355	$\angle(H_4C_2H_1)$	118.3
		$r(H_4C_2)$	1.075	$\omega(H_2C_1OH_1)$	114.2
				$\omega(H_4C_2H_1O)$	89.3

[a] See Figure 2 for the numbering of atoms. Bond distance (r) is given in Å and angle in deg. ω means dihedral angle. H', the equivalent atom to H. SP, saddle point. IM, intermediate. The STO-3G optimized structures are very similar to those of 6-31G** except that C–O and O–H distances are a little longer in STO-3G, e.g., 1.433 and 0.991 Å in methanol, respectively.

where $a = (^1/_2)(E_T/C)^{1/2}$, $b = (^1/_2)[(E_T + \Delta H)/C]^{1/2}$, $d = (^1/_2)[(P^2 - C)/C]^{1/2}$, and $C = h^2/8\mu L$. μ is the mass of the representative point whose value is unity in the mass-weighted $3N - 6$ dimensional Cartesian coordinates.

Using the $P(E_T)$ of formula 2, the value proportional to the rate constant $K(T)$ along the IRC path can be calculated by formula 3 when a Boltzmann distribution is assumed for the translational energy of the representative point at a temperature T

$$K(T) \propto \int_0^\infty P(E_T) \exp(-E_T/kT) \, dE_T \qquad (3)$$

where k is the Boltzmann constant.[19,20,21]

The classical rate constant is also calculated by formula 3 with $P^{CL}(E_T)$ of formula 4 instead of formula 2[19,20,21]

$$\begin{aligned} P^{CL}(E_T) &= 0 \qquad E_T < V(Q_m) \\ P^{CL}(E_T) &= 1 \qquad E_T \geq V(Q_m) \end{aligned} \qquad (4)$$

In this case formula 3 becomes formula 5, the familiar rate constant expression.

$$K(T) \propto kT \exp(-V(Q_m)/kT) \qquad (5)$$

The results using (3) and (5) are collected in Figure 3.

Tentatively assuming that the total contribution to the rate constant from other normal coordinates of the potential energy hypersurface have a similar value in each type of reactions, the insertion in the singlet state and the abstraction in the triplet state, the relative rate constants theoretically obtained along the IRC paths, which are shown in Figure 3, are approximately proportional to the percent yields of the reaction products in the experiments. If the contribution of the triplet carbene dominates at low temperatures as proposed by Platz[3] and Izawa,[1,2] the main product is always ether regardless of the temperature in both the classical and the tunneling mechanisms, i.e., there is no temperature-dependent product variation in this case. On the other hand, if singlet carbene plays a main role even at low temperatures, the representative point of the insertion reaction of the O–H bond will be effectively trapped at the bottom of the potential energy hypersurface of the intermediate (Figure 1a) at low temperatures; i.e., the insertion reaction into the O–H bond will diminish remarkably at low temperatures. In Figure 3, there are two kinds of rate
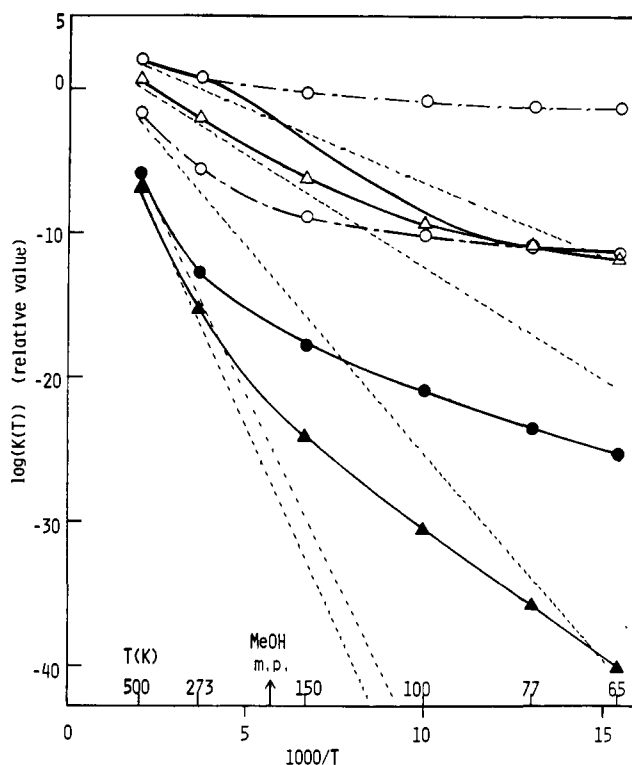
(21) M. A. Eliason and J. O. Hirschfelder, *J. Chem. Phys.*, **30**, 1426 (1959).

Figure 3. Rate constants of the reaction along the IRC path: (---) classical mechanism assumed; (—) tunneling mechanism assumed; O, O–H insertion (the upper is effective at high temperatures and the lower at low temperatures); △, C–H insertion; ●, O–H abstraction; ▲, C–H abstraction.

constant curves for the insertion reaction of the O–H bond, one of which was calculated under the condition that the activation energy $V(Q_m)$ is measured from the reactant and the other from the intermediate. The former curve is effective in the reaction at high temperatures and the latter in that at low temperatures. The transition from the former curve to the latter may take place gradually near the melting point of the solvent. Therefore, at high temperatures the insertion of singlet carbene into the O–H bond predominates in contrast to the insertion to the C–H bond, even though there are three C–H bonds in methanol compared with one O–H bond, but the situation changes to the preponderance of the insertion into the C–H bond at low temperatures. The same
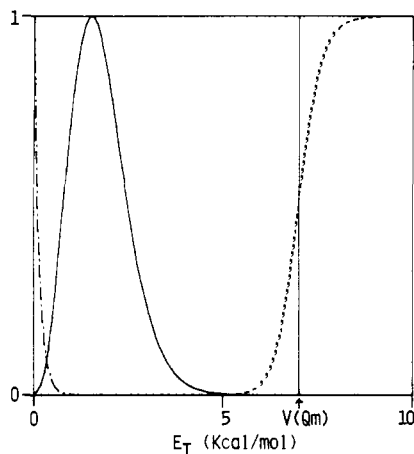
Figure 4. Kinetic energy dependence of the contribution of the representative point for the rate constant of O–H insertion at 77 K. Abcissa: Kinetic energy of the representative point. Ordinate: The normalized values of the tunneling probability $P(E_T)$ (---), Boltzmann distribution $\exp(-E_T/kT)$ (···), and their product $P(E_T) \exp(-E_T/kT)$ (—). The normalization was carried out such that the maximum of each of these values is 1. The reaction rate constant is obtained by the integration of the area below the solid curve (see formula 3).

conclusion is obtained by the classical mechanism as well as the tunneling mechanism (Figure 3). However, the very low activation energy at low temperatures[2,3,9] can be explained by the tunneling mechanism only as found in Figure 3.

The isotope effect in tunneling is explained by the increase of the effective thickness of the potential energy barrier along the IRC path as well as the increase of the effective barrier height.[22] Recent observations of the isotope effect in the same reaction at

low temperature[23] may be explained by the treatment considering these origins.

Contribution of Hydrogen Atom Displacement to the Tunneling Effect. The unique normal mode of vibration of imaginary frequency at the saddle point is shown in Figure 2 for each of the reactions investigated. It is interesting that the normal mode of vibration of imaginary frequency is the displacement of the bridged hydrogen atom only in all of the reactions.

Le Roy used the mass of the hydrogen atom being abstracted as the effective reduced mass of the reacting system $\cdot CH_3 + CH_3CN \rightarrow CH_4 + \cdot CH_2CN$ in tunneling.[6] Brunton et al. used the same treatment in their publication.[9] If the bridged hydrogen atom displacement only would be the main contribution to tunneling also in the present research, the tunneling passing through the energy barrier must be done by the representative point whose translational energy is nearly equal to $V(Q_m)$, because the main contribution of the bridged hydrogen atom displacement is only effective near Q_m in Figure 1. However, this consideration is wrong as is clearly shown in Figure 4, as an example, where the main contribution to the rate constant is due to the tunneling of the representative point whose translational energy is very low. This means that the reaction system follows approximately the whole structure change along the IRC path even when the tunneling takes place at the low temperature; i.e., the displacements of not only the bridged hydrogen atom but also all of the atoms constructing the reaction system contribute to the tunneling as well as to the classical mechanism.

Registry No. Methylene, 2465-56-7; methanol, 67-56-1.

(22) M. Tsuda, S. Oikawa, and K. Nagayama, Symposium on Photochemistry (Japanese), 1983, Tsukuba (1983), p 369.

(23) H. Tomioka, Y. Ozaki, and Y. Izawa, *Bull. Chem. Soc. Jpn.*, **56**, 1239 (1983).

Solid-State NMR of Cyclic Pentapeptides

M. H. Frey,[†] S. J. Opella,*[†] A. L. Rockwell,[‡] and L. M. Gierasch*[‡]

Contribution from the Departments of Chemistry, University of Pennsylvania, Philadelphia, Pennsylvania 19104, and University of Delaware, Newark, Delaware 19711. Received July 23, 1984

Abstract: The structure and dynamics of several cyclic pentapeptides with well-defined conformational features are described by solid-state NMR spectroscopy. Isotropic chemical shift spectra for solution and polycrystalline samples are compared. The dynamics of phenyl ring side chains are described with line-shape analysis of both high-resolution spectra and powder patterns. The bond lengths of N–H groups involved in intramolecular hydrogen bonds are measured.

Solid-state NMR spectroscopy is an effective way to describe the structural and dynamical properties of crystalline and amorphous solid biological molecules.[1] NMR studies provide structural information that is complementary to that obtained from diffraction studies. For those molecules that do not form single crystals or are insoluble, solid-state NMR spectroscopy provides one of the few ways of studying these molecules at high resolution. For those molecules that form single crystals suitable for X-ray or neutron diffraction studies, solid-state NMR spectroscopy

provides unique dynamical information and complementary structural information. Synthetic cyclic peptides serve as interesting and convenient model systems for exploring applications of solid-state NMR to biological systems. The general spectroscopic approach is appropriate for essentially any medium-sized molecule, and some features of it can be extended to macromolecules. We have concentrated on polycrystalline samples; although alternative strategies that utilize the spectroscopic properties of single crystals are in some cases more powerful, they

[†] University of Pennsylvania.
[‡] University of Delaware.

(1) Opella, S. J. *Annu. Rev. Phys. Chem.* **1982**, *33*, 533–562.